Priority Report

Cancer Research

HDAC6 Inhibition Synergizes with Anti-PD-L1 Therapy in ARID1A-Inactivated Ovarian Cancer

Takeshi Fukumoto[1], Nail Fatkhutdinov[1], Joseph A. Zundell[1], Evgenii N. Tcyganov[2], Timothy Nacarelli[1], Sergey Karakashev[1], Shuai Wu[1], Qin Liu[3], Dmitry I. Gabrilovich[2], and Rugang Zhang[1]

Abstract

ARID1A, encoding a subunit of the SWI/SNF complex, is the most frequently mutated epigenetic regulator in human cancers and is mutated in more than 50% of ovarian clear cell carcinomas (OCCC), a disease that currently has no effective therapy. Inhibition of histone deacetylase 6 (HDAC6) suppresses the growth of *ARID1A*-mutated tumors and modulates tumor immune microenvironment. Here, we show that inhibition of HDAC6 synergizes with anti-PD-L1 immune checkpoint blockade in ARID1A-inactivated ovarian cancer. ARID1A directly repressed transcription of *CD274*, the gene encoding PD-L1. Reduced tumor burden and improved survival were observed in $ARID1A^{flox/flox}/PIK3CA^{H1047R}$ OCCC mice treated with the HDAC6 inhibitor ACY1215 and anti-PD-L1 immune checkpoint blockade as a result of activation and increased presence of IFNγ-positive CD8 T cells. We confirmed that the combined treatment limited tumor progression in a cytotoxic T-cell–dependent manner, as depletion of $CD8^+$ T cells abrogated these antitumor effects. Together, these findings indicate that combined HDAC6 inhibition and immune checkpoint blockade represents a potential treatment strategy for *ARID1A*-mutated cancers.

Significance: These findings offer a mechanistic rationale for combining epigenetic modulators and existing immunotherapeutic interventions against a disease that has been so far resistant to checkpoint blockade as a monotherapy.

See related commentary by Prokunina-Olsson, p. 5476

Introduction

ARID1A encodes a subunit of the SWI/SNF chromatin–remodeling complex and functions as a tumor suppressor (1). SWI/SNF complexes are multi-subunit complexes that remodel chromatin in an ATP-dependent manner (1). In addition to core subunits such as SNF5 that are present in all SWI/SNF complexes, other subunits are only present in certain complexes. For example, the mutually exclusive ARID1A and ARID1B subunits are only associated with BRG1-associated factor (BAF) complexes, while ARID2, PBRM1, and BRD7 subunits are specific for polybromo BAF (PBAF) complexes (1). The ARID1A containing SWI/SNF complex epigenetically activates or represses gene expression via controlling gene accessibility (1, 2).

ARID1A is among the most frequently mutated genes in human cancer (3). In addition to inactivating mutations, *ARID1A* shows deletions in many tumor types in the cBioPortal datasets. Notably, inactivating mutations in *ARID1A* occur frequently in ovarian clear cell carcinomas (OCCC; >50%; ref. 4). Over 90% of *ARID1A* mutations in OCCCs are either frameshift or nonsense that led to loss of ARID1A protein expression (4). There is an unmet need for effective treatment modalities for *ARID1A*-mutated OCCCs. OCCC is generally refractory to standard agents used to treat ovarian cancers, and when diagnosed in advanced stages, OCCC carries the worst prognosis of all ovarian cancer histosubtypes (5).

Emerging evidence supports the idea that the SWI/SNF complexes play a critical role in tumor immunity (2). For example, in the SWI/SNF catalytic subunit *SMARCA4*-mutated small-cell carcinoma of the ovary, hypercalcemic type (SCCOHT), PD-L1 is expressed in both tumor and stromal cells, and strong T-cell infiltration was observed in the majority of tumors (6). Emerging clinical evidence suggests that checkpoint blockades such as anti-PD1 are effective in SCCOHTs (6). In addition, in clear cell renal cell cancer, patients who responded positively to anti-PD1/anti-PD-L1 therapy often carry a loss of function mutation in the *PBRM1* subunit of the PBAF complex (7). Likewise, inactivation of the PBAF subunits BRD7, ARID2, and PBRM1 confers susceptibility to T-cell–mediated killing in melanoma (8). Finally, *ARID1A* mutation correlates with an increase of PD-L1 expression (9). However, the mechanism by which ARID1A regulates PD-L1 expression remains not fully understood. Notably, published literature show that anti-PD-L1 treatment only has a modest effect on improving the survival of mice bearing ARID1A-inactivated tumors (9). This suggests that checkpoint blockade–based combination therapeutic strategies are necessary for treating *ARID1A*-mutated cancers.

The tumor microenvironment contains a variety of immune modulating cells such as T lymphocytes (10, 11). These cells play a critical role in shaping the immune response against tumors. Therefore, agents that promote functional changes in

[1]Gene Expression and Regulation Program, The Wistar Institute, Philadelphia, Pennsylvania. [2]Immunology, Microenvironment & Metastasis Program, The Wistar Institute, Philadelphia, Pennsylvania. [3]Molecular and Cellular Oncogenesis Program, The Wistar Institute, Philadelphia, Pennsylvania.

Note: Supplementary data for this article are available at Cancer Research Online (http://cancerres.aacrjournals.org/).

Corresponding Author: Rugang Zhang, Wistar Institute, 3601 Spruce Street, Philadelphia, PA, 19104. Phone: 215-495-6840; Fax: 215-898-3792; E-mail: rzhang@wistar.org

Cancer Res 2019;79:5482–9

doi: 10.1158/0008-5472.CAN-19-1302

©2019 American Association for Cancer Research.

Downloaded from http://aacrjournals.org/cancerres/article-pdf/79/21/5482/2871694/5482.pdf by guest on 04 December 2023

T cells may alter immune microenvironment to affect tumor progression (11). HDAC6 inhibition suppresses the growth of *ARID1A*-mutated cancer (12). Although most translational studies on HDAC6 inhibitors have focused on their effects on tumor cells, emerging evidence suggests that HDAC6 inhibitors have immunomodulatory effects on tumor immune microenvironment (13–15). Notably, the complete genetic knockout of HDAC6 does not impair normal cell function (16). Consistently, the clinically applicable HDAC6 inhibitor ACY1215 was proven safe (17).

Here we show that ARID1A represses *CD274* (encoding PD-L1) gene and HDAC6 inhibition synergizes with anti-PD-L1 in ARID1A-inactivated ovarian cancer. The combination depends on cytotoxic T-cell activity to limit tumor progression *in vivo*. Our findings establish that HDAC6 inhibition and immune checkpoint blockade combination represents a treatment strategy for *ARID1A*-mutated cancers.

Materials and Methods

Cell lines and culture conditions

The OCCC cell line OVCA429 and mouse ovarian ID8-*Defb29*/*Vegf* cancer cells were cultured in RPMI1640 (Corning Life Sciences) supplemented with 10% FBS (Sigma-Aldrich) and 1% penicillin/streptomycin. The OCCC cell line RMG1 was cultured in 1:1 DMEM/F12 (Corning Life Sciences) supplemented with 10% FBS and 1% penicillin/streptomycin. RMG1 cells were obtained from the Japanese Collection of Research Bioresources in 2015. OVCA429 cells were obtained from I.M. Shih (Johns Hopkins University, Baltimore, MD) in 2015. ID8-*Defb29*/*Vegf* cells were obtained from J.R. Conejo-Garcia (H. Lee Moffit Cancer Center, Tampa, FL) in 2015. All cells were used within 10 passages. The viral packaging Phoenix and 293FT cells were cultured in DMEM (Corning Life Sciences) supplemented with 10% FBS and 1% penicillin/streptomycin. All cells were incubated at 37°C in humidified atmosphere containing 5% CO_2. Cell lines were authenticated at the Wistar Institute Genomics Facility using short tandem repeat profiling using AmpFLSTR Identifiler PCR Amplification Kit (Life Technologies) right before experiments. *Mycoplasma* infection was monthly tested with LookOut Mycoplasma PCR Detection (Sigma-Aldrich) right before experiments.

Quantitative reverse-transcriptase PCR

Total RNA was extracted using TRIzol (Invitrogen), and then purified with DNase treatment (Qiagen). RNA expression was determined using the QuantStudio 3 Real-Time PCR System (Thermo Fisher Scientific) and iTaq Universal SYBR Green One-step Kit (Bio-Rad Laboratories). The primers sequences are as following: human *CD274* (forward, 5'-ATGGTGGTGCCGACTACAA-3'; reverse, 5'-TCCAGATGACTTCGGCCTT-3') and mouse *Cd274* (forward, 5'-GCCACTTCTGAGCATGAACTA-3'; reverse, 5'-GACACTTCTCTTCCCACTCAC-3'). The expression was normalized using human *18s* (forward, 5'-AACTTTCGATGGTAGTCGCCG-3'; reverse, 5'-CCTTGGATGTGGTAGCCGTTT-3') expression, or mouse *Ppia* (forward, 5'-GGGTTCCTCCTTTCACAGAA-3'; reverse, 5'- GATGCCAGGACCTGTATGCT-3').

Reagents and antibodies

ACY1215 (catalog no. S8001) was purchased from Selleckchem. Anti-PD-L1 (catalog no. BE0101, clone: 10F.9G2) and anti-mouse CD8 (catalog no. BE0117, clone: YTS 169.4) antibodies were purchased from Bio X Cell. IFNγ was purchased from Thermo Fisher Scientific (catalog no. PHC4031) or from ProSpec (catalog no. CYT-358). The following antibodies were purchased from the indicated suppliers: rabbit anti-ARID1A (Cell Signaling Technology, catalog no. 12354, 1:1000), rabbit anti-ARID1B (Cell Signaling Technology, catalog no. 92964, 1:1000), mouse anti-ARID1B (Santa Cruz Biotechnology, catalog no. sc-32762, 1:1000), mouse anti-β-actin (Sigma-Aldrich, catalog no. A5441, 1:10,000), mouse anti-FLAG (Sigma-Aldrich, catalog no. F1804), rabbit anti-PD-L1 (Cell Signaling Technology, catalog no. 13684S, 1:1000; Abcam, catalog no. ab213480, 1:1000). For flow cytometric analysis, APC/CY7 anti-CD69 (catalog no. 104525), BV711 anti-CD3 (catalog no. 100349), APC anti-CD4 (catalog no. 100516), PE anti-CD8 (catalog no. 100708), FITC anti-granzyme B (catalog no. 372206), PE/Cy7 anti-IFNγ (catalog no. 505825) antibodies were purchased from BioLegend and used at 1:150 dilutions. Anti-FOXP3 antibody (catalog no. 563902, 1:150) was purchased from BD Biosciences. Zombie yellow dye (BioLegend, catalog no. 423103, 1:200) was used as a viability staining.

Immunoblotting

Protein was isolated using RIPA buffer (50 mmol/L Tris pH 8.0, 150 mmol/L NaCl, 1% Triton X-100, 0.5% sodium deoxycholate and 1 mmol/L PMSF). The concentrations of protein samples were measured using Bradford assay. Protein samples were separated by SDS-PAGE gel and transferred to polyvinylidene fluoride membrane (Millipore). Membranes were blocked in TBS/0.1% Tween 20 with 5% non-fat milk (Bio-Rad), and then incubated sequentially with primary and secondary antibodies.

Generation of endogenously FLAG-tagged ARID1A and ARID1A knockout cells by CRISPR

To generate endogenously FLAG-tagged ARID1A, PX458 (Addgene #48138) and pFETCh-donor (Addgene #63934) constructs were obtained from Addgene. Guide RNA sequence (5'-TGTCCCACGGCTGTCATGAC-3') targeting terminal codon of ARID1A was inserted into PX458. About 500 bps homologous arms at both sides of guide RNA–targeting site were cloned and inserted into pFETCh donor. ARID1A endogenously tagged clones were isolated after 200 μg/mL G418 selection and validated by immunoblot.

ARID1A knockout (ARID1A KO) cells were generated and validated as reported previously (12). For all the controls, parental cells transduced with empty vector packaged virus were used. Briefly, OVCA429 cells were transfected with pSpCas9 (BB)-2A-Puro (PX459) (Addgene, catalog no. 62988) inserting the *ARID1A* guide RNA (5'-CGGGTTGCCCAGGCTGCTGGCGG-3'). ID8-*Defb29/Vegf* cells were transfected with lentiCRISPR v2 (Addgene, catalog no. 52961) inserting the *Arid1a* guide RNA (5'-CACCGTCTCCGCGGACGAGACAGCG-3'). Lipofectamine 2000 was used following the manufacturer's specifications then selection using 1 μg/mL puromycin was performed. Fugene6 transfection reagent (Promega) was used following the manufacturer's specifications then selection using 1 μg/mL puromycin was performed. Clonal populations for ARID1A KO were screened using immunoblotting.

Flow cytometry

PD-L1 expression on the cell surface was analyzed as we described previously (18). Briefly, cells were harvested and washed in PBS. Cells were then centrifuged and incubated in 100 μL FACS

Downloaded from http://aacrjournals.org/cancerres/article-pdf/79/21/5482/2871694/5482.pdf by guest on 04 December 2023

buffer (PBS with 3% FBS) with 1:100 diluted PE anti-human CD274 (BD Biosciences, catalog no. 557924, clone: MIH1) or APC anti-mouse Cd274 (BioLegend, catalog no. 124311, clone: 10F.9G2) for 40 minutes on ice. Cells were then stained with 100 μL FACS buffer with 1:5 diluted 7AAD (BD Pharmingen, catalog no. 51-68981E) for 10 minutes on ice. Cells were washed with PBS, suspended in 400 μL PBS, and then submitted for analysis. At least 20,000 events were collected on flow cytometry, and then the data were analyzed with FlowJo version 7 software module. An isotype-matched IgG was used as a negative control.

Tumor cells were extracted using enzymatic cocktail from Mouse Tumor Dissociation Kit (Miltenyi Biotec, catalog no. 130-096-730) according to the manufacturer's instructions. After dissociation, cells were mashed through a 70-μm cell strainer and used for flow cytometric analysis. For peritoneal wash, peritoneal cavity of mice was washed three times with 5 mL PBS and incubated in red blood cell lysis buffer before proceeding to staining.

Intracellular IFNγ staining was performed by culturing tumor cell suspensions or peritoneal washes with protein transport inhibitor (BD Biosciences, catalog no. 554724) and stimulated with phorbol 12-myristate 13-acetate (Sigma, catalog no. P8139, 0.5 μg/mL) and ionomycin (Sigma, catalog no. I0634, 1 μg/mL) for 24 hours followed by surface and viability staining. Cells were fixed and permeabilized using Cytofix/Cytoperm Kit (BD Biosciences, catalog no. 554714) according to the manufacturer's instructions followed by intracellular staining.

Chromatin immunoprecipitation and CUT&RUN analysis

For chromatin immunoprecipitation (ChIP) analysis, cells were cross-linked with 1% formaldehyde, and the reaction was quenched by 125 mmol/L glycine. Fixed cells were lysated using lysis buffer 1 (50 mmol/L HEPES-KOH, pH 7.5, 140 mmol/L NaCl, 1 mmol/L EDTA, pH 8.0, 1% Triton X-100, 0.1% DOC) and lysis buffer 2 (10 mmol/L Tris pH 8.0, 200 mmol/L NaCl, 1 mmol/L EDTA, 0.5 mmol/L EGTA). Samples were digested with MNase in digestion buffer (10 mmol/L Tris 8.0, 1 mmol/L $CaCl_2$, 0.2% Triton X-100) and the nucleus was broken down using one pulse of bioruptor with high output. Chromatin was incubated with antibodies overnight, and then protein A+G Dynabeads were added. After 1.5 hours incubation, chromatin was eluted, treated with proteinase K, and then purified with a Gel Extraction Kit (Qiagen, catalog no. 28706). The following antibodies were used to perform ChIP: rabbit anti-SNF5 (Bethyl, catalog no. A301-087A), mouse anti-ARID1B (Abgent, catalog no. AT1190a), rabbit anti-ARID1B (Cell Signaling Technology, catalog no. 92964), rabbit anti-H3K4me3 (Active Motif, catalog no. 39159), mouse anti-RNA polymerase II (Santa Cruz Biotechnology, catalog no. sc-47701), and mouse anti-FLAG (Sigma-Aldrich, catalog no. F1804). An isotype-matched IgG was used as a negative control. ChIP DNA samples were analyzed by quantitative PCR against the promoter of the human *CD274* gene (forward, 5'-GCCGATTTCACC-GAAGGTC-3'; reverse, 5'-CAGCTGCTCAGCGTTGC-3') or of the mouse *Cd274* gene (forward, 5'-GCCACTTCTGAGCATGAACTA-3'; reverse, 5'-GACACTTCTCTTCCCACTCAC-3').

CUT&RUN for ARID1A's association with the *CD274* promoter analysis was performed as we described previously (19). Briefly, cells were washed with Wash Buffer [20 mmol/L HEPES pH 7.5, 150 mmol/L NaCl, 0.5 mmol/L spermidine and a Roche complete EDTA-free tablet (Sigma-Aldrich) per 50 mL] and centrifuged. Cell pellets were incubated in Antibody Buffer (antibody with 1:100 dilution in wash buffer supplemented with 0.05% digitonin and 2 mmol/L EDTA) for 2 hours. After centrifugation, cell pellets were washed with Dig-Wash Buffer (Wash Buffer with 0.05% digitonin), and incubated in Protein A-MNase at a final concentration of 700 ng/mL in Dig-Wash Buffer for 1 hour. Cells were suspended in 100 μL Dig-Wash Buffer, and then mixed with 2 μL 100 mmol/L $CaCl_2$. After 30-minute incubation, reactions were stopped using STOP buffer (340 mmol/L NaCl, 20 mmol/L EDTA pH 8, 4 mmol/L EGTA, 0.05% digitonin, 50 μg/mL RNase A, 50 μg/mL glycogen), then centrifuged. The supernatant containing DNA was collected and purified using phenol–chloroform–isoamyl alcohol and chloroform extraction and ethanol precipitation. Rabbit anti-ARID1A (Abcam, catalog no. ab182560) was used to perform CUT&RUN. An isotype-matched IgG was used as a negative control. CUT&RUN DNA samples were analyzed by quantitative PCR against the promoter of the human *CD274* gene (forward, 5'-GCCGATTTCACC-GAAGGTC-3'; reverse, 5'-CAGCTGCTCAGCGTTGC-3') or of the mouse *Cd274* gene (forward, 5'-GCCACTTCTGAGCATGAACTA-3'; reverse, 5'-GACACTTCTCTTCCCACTCAC-3').

Arid1a$^{-/-}$/*Pik3ca*^{H1047R} genetic OCCC mouse model

All experimental protocols were approved by the Wistar Institutional Animal Care and Use Committee (IACUC). The transgenic mice were generated as we described previously (12). Briefly, *Arid1a*$^{flox/flox}$ mice (kindly provided by Dr. Wang, University of Michigan, Ann Arbor, MI) were crossed with *R26-Pikca*^{H1047R} mice (Jackson Laboratory, Jax no. 016977). Intrabursal adenovirus-Cre injection was used to induce OCCC formation. Mice were randomized into four groups 4 weeks after adeno-Cre injection and treated with vehicle control (isotype control IgG and 2% DMSO/30% PEG 300/ddH_2O), ACY1215 (50 mg/kg, daily), anti-PD-L1 antibody (10 mg/kg, twice a week), or a combination for 21 days. ACY1215 was suspended in 2% DMSO/30% PEG 300/ddH_2O, and anti-PD-L1 antibody was suspended in PBS. At the end of treatments, mice were euthanized and tumors were surgically dissected, or followed for survival analysis. Tumor burden was calculated on the basis of tumor weight. The Wistar Institute IACUC guideline was followed in determining the time for ending the survival experiments (tumor burden exceeds 10% of body weight).

In vivo CD8 T-cell depletion

An anti-CD8 antibody (BioXCell, catalog no. BE0117, clone: YTS 169.4, 10 mg/kg) was used to deplete $CD8^+$ T cells. An isotype-matched IgG (Bio X Cell, catalog no. BE0090, clone: LTF-2, 10 mg/kg) was used as a negative control. Antibodies were administered 3 days before starting the combination treatment and then twice a week until completion of the study. The depletion was confirmed by flow cytometry analysis of blood cells collected via the retro-orbital vein.

Statistical analysis and reproducibility

Statistical analysis was conducted using GraphPad Prism 6 Software (GraphPad). Experiments were performed in three independent experiments unless otherwise stated and representative results were shown. Quantitative data are expressed as mean ± SEM unless otherwise stated. To improve data normality and homogeneity of variance, some data (e.g., tumor weight, ascites, and percent of specific cell counts) were log-transformed before statistical test. A two-tailed *t* test was conducted for two group comparison. ANOVA with *post hoc* Tukey multiple comparisons test was used for experiment with four

Downloaded from http://aacrjournals.org/cancerres/article-pdf/79/21/5482/2871694/5482.pdf by guest on 04 December 2023

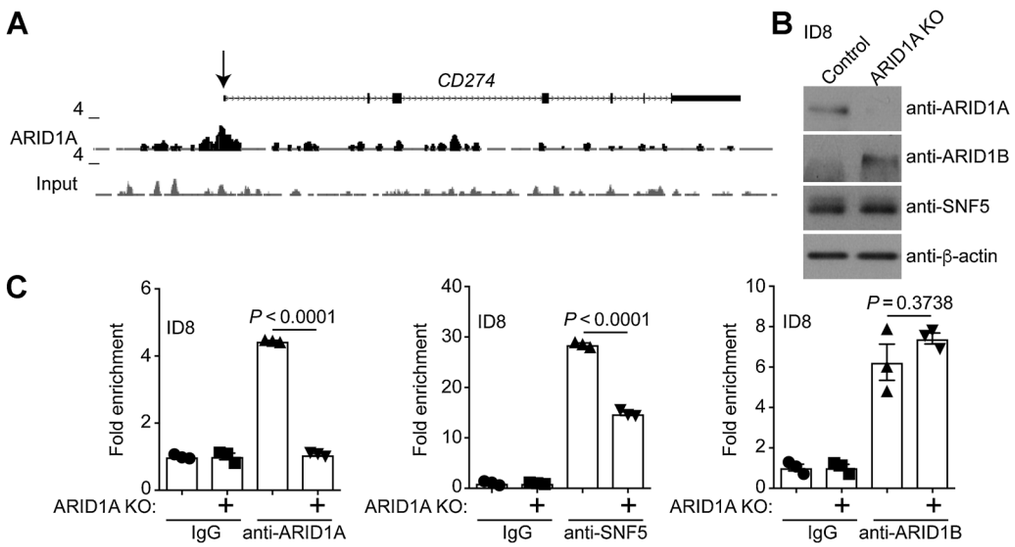

Figure 1.

CD274 is a direct ARID1A target gene. **A,** ARID1A ChIP-seq track on the *CD274* gene locus in *ARID1A* wild-type RMG1 cells. **B,** Expression of ARID1A, ARID1B, SNF5, and β-actin in the *ARID1A* wild-type control and ARID1A KO mouse ovarian ID8-*Defb29/Vegf* cells. **C,** The indicated ID8-*Defb29/Vegf* cells were subjected to ChIP analysis for the association of the indicated proteins with the *Cd274* gene promoter using the indicated antibodies against ARID1A, SNF5, ARID1B, or an isotype-matched IgG control. Error bars, ± SEM. $n = 3$ independent experiments.

independent groups. For experiment with eight independent groups, ANOVA with *post hoc* multiple *t* tests and Benjamini and Hochberg adjusted *P* values were reported. $P < 0.05$ was considered significant.

Data availability

Previously published ARID1A ChIP-seq in ARID1A wild-type RMG1 cells are available at the Gene Expression Omnibus under access code GSE104545.

Results

CD274 is a direct ARID1A target gene

ARID1A ChIP followed by next-generation sequencing (ChIP-seq) analysis revealed that ARID1A was associated with the PD-L1 encoding *CD274* gene promoter in *ARID1A* wild-type OCCC cells (Fig. 1A; ref. 20). We validated the binding of ARID1A to the *Cd274* gene promoter by ChIP in the mouse ovarian ID8-*Defb29/Vegf* cells (Fig. 1B and C) in which PD-L1 is implicated (18). As a negative control, ARID1A binding to the *Cd274* promoter was reduced to a level observed in IgG controls in ARID1A KO ID8-*Defb29/Vegf* cells (Fig. 1C). Notably, SNF5, a core subunit of the SWI/SNF complex, was also associated with the *Cd274* promoter and its association was reduced by ARID1A KO (Fig. 1C). Expression of ARID1B, the mutually exclusive subunit of the SWI/SNF complex with ARID1A, was upregulated in ARID1A KO ID8-*Defb29/Vegf* cells (Fig. 1B; ref. 21). Although ARID1B was also associated with the *Cd274* promoter, ARID1A KO did not affect the association of ARID1B with the *Cd274* promoter (Fig. 1C). This suggests that ARID1B is unable to compensate for ARID1A loss on the *Cd274* promoter. Similar observations were also made in the *ARID1A* wild-type human OCCC cell lines OVCA429 and RMG1 (Supplementary Fig. S1), indicating that the association of ARID1A with the *CD274* promoter is not a cell line–specific effect. Together, we conclude that *CD274* is a direct ARID1A target gene.

ARID1A represses *CD274* gene transcription

We next determined the effect of ARID1A status on changes in *Cd274* mRNA and PD-L1 expression. Compared with *ARID1A* wild-type control ID8-*Defb29/Vegf* cells, *Cd274* mRNA was increased by ARID1A KO (Fig. 2A). Consistently, PD-L1 expression measured by both immunoblot and FACS analysis was upregulated upon ARID1A KO (Fig. 2A). IFNγ plays a major role in inducing PD-L1 expression (22). Thus, we examined the effects of ARID1A KO on IFNγ-induced PD-L1 expression. ARID1A KO significantly enhanced the upregulation of *Cd274* mRNA and PD-L1 expression induced by IFNγ treatment (Fig. 2A). Similar findings were made in both *ARID1A* wild-type mouse ID8-*Defb29/Vegf* cells and human OVCA429 and RMG1 cells with or without ARID1A KO (Supplementary Fig. S2). We next examined the association of RNA polymerase II (Pol II) and lysine 4 trimethylated histone H3 (H3K4me3), a transcription active promoter epigenetic mark, with the *Cd274* promoter. Consistent with changes observed in *Cd274* mRNA and PD-L1 expression, ARID1A KO enhanced the association of Pol II and H3K4me3 with the *Cd274* promoter with or without IFNγ stimulation (Fig. 2B). Together, we conclude that ARID1A represses *CD274* gene transcription at both the basal levels and in response to IFNγ stimulation.

Combination of HDAC6 inhibitor and anti-PD-L1 in the *ARID1A*$^{flox/flox}$/*PIK3CA*^{H1047R} OCCC mouse model

Given HDAC6 inhibitors' role in immune modulation (13–15), we examined the effects of HDAC6 inhibitor ACY1215 in a conditional genetic *ARID1A*$^{flox/flox}$/*PIK3CA*^{H1047R} OCCC mouse model (Supplementary Fig. S3A; refs. 12, 23). Notably, HDAC6 inhibitor ACY1215 significantly increased the CD69^{+}-activated CD4 and CD8 T cells in the peritoneal wash

Downloaded from http://aacrjournals.org/cancerres/article-pdf/79/21/5482/2871694/5482.pdf by guest on 04 December 2023

(Supplementary Fig. S3B). Consistently, IFNγ$^+$ CD4 and CD8 T cells were also significantly increased by ACY1215 treatment (Fig. 3A). In contrast, ACY1215 did not significantly affect Granzyme B$^+$ CD8 T cells or Foxp3$^+$ regulatory T cells (Supplementary Fig. S3C). These findings suggest that HDAC6 inhibition may boost antitumor immunity. However, a combination of ACY1215 and anti-PD-L1 treatment only increased IFNγ$^+$ CD8, but not CD4 T cells (Fig. 3A). This suggests the implication of CD8 T cells in the combination treatment.

Because ARID1A directly represses PD-L1 and HDAC6 inhibition increases T-cell activation and activity, we sought to determine the effects of HDAC6 inhibitor ACY1215 and anti-PD-L1 combination in ARID1A-inactivated OCCCs. Toward this goal, we first establish OCCCs in 6–8 weeks old *ARID1A*$^{flox/flox}$/*PIK3CA*^{H1047R} female mice by intrabursally injecting adenovirus-Cre (12). Four weeks after the adenovirus-Cre injection, the mice were randomized into four treatment groups: (i) vehicle and IgG control; (ii) ACY1215 (50 mg/kg daily by i.p.) and IgG control; (iii) vehicle control and anti-PD-L1 antibody (10 mg/kg twice weekly by i.p.); and (iv) ACY1215 and anti-PD-L1 antibody combination for an additional 3 weeks. At the end of treatment, orthotopic tumors were surgically removed (Fig. 3B). The tumor weight was measured as a surrogate for tumor burden. As reported previously (9, 12), both anti-PD-L1 antibody and ACY1215 significantly reduced the tumor weight in the OCCC model (Fig. 3B). We also examined effects of the ACY1215 and anti-PD-L1 combination in reducing ascites produced in the *Arid1a*$^{flox/flox}$/*Pik3ca*^{H1047R} OCCC model. Both ACY1215 and anti-PD-L1 single treatment significantly reduced the amount of ascites produced in this model (Fig. 3C). The reduction in tumor weight and ascites production by ACY1215 or anti-PD-L1 single treatment correlated with an improvement of survival (Fig. 3D). The HDAC6 inhibitor ACY1215 and anti-PD-L1 combination was synergistic in reducing the tumor burden and improving the survival of tumor-bearing mice (Fig. 3B and D). Notably, the combination completely eliminated the ascites production (Fig. 3C). The doses of ACY1215 and anti-PD-L1 used in this study did not significantly affect the body weight of treated mice (Supplementary Fig. S3D), suggesting that effective combination doses can be achieved without gross toxicity. Together, we conclude that HDAC6 inhibitor ACY1215 and anti-PD-L1 are synergistic in reducing tumor burden, which correlated with an improvement of survival of mice bearing ARID1A-inactivated OCCCs.

CD8$^+$ T-cell depletion abrogates the antitumor effects of ACY1215 and anti-PD-L1 combination

Because ACY1215 and anti-PD-L1 combination increases IFNγ$^+$ CD8, but not CD4, T cells (Fig. 3A) and cytotoxic CD8 T cells play a critical role in mediating the antitumor effects of anti-PD-L1 treatment (10), we next sought to determine whether the combination limits the progression of *ARID1A*-mutated OCCCs through CD8 T cells. Toward this goal, we depleted CD8 T cells by treating the combination-treated mice with an anti-CD8 antibody (Fig. 4A). Compared with IgG control–treated mice, anti-CD8

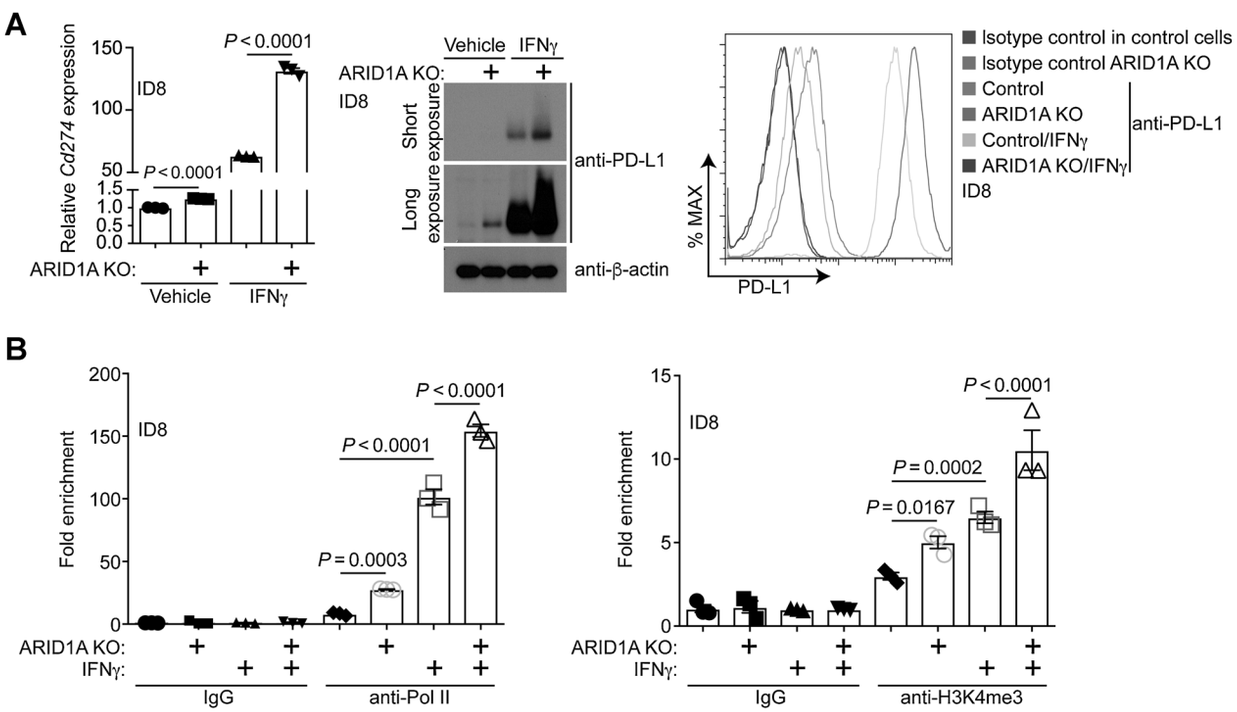

Figure 2.

ARID1A transcriptionally represses *Cd274*. **A,** Expression of *Cd274* mRNA and PD-L1 protein in *ARID1A* wild-type control and ARID1A KO mouse ovarian ID8-*Defb29/Vegf* cells treated with or without 20 ng/mL IFNγ determined by quantitative reverse-transcriptase PCR (left) or immunoblot (middle). Right, the cell surface expression of PD-L1 in these cells was determined by flow cytometry analysis. **B,** The indicated ID8-*Defb29/Vegf* cells treated with or without 20 ng/mL IFNγ cells were subjected to ChIP analysis for the *Cd274* gene promoter using the indicated antibodies or an isotype-matched IgG control. Error bars, ± SEM. n = 3 independent experiments.

Downloaded from http://aacrjournals.org/cancerres/article-pdf/79/21/5482/2871694/5482.pdf by guest on 04 December 2023

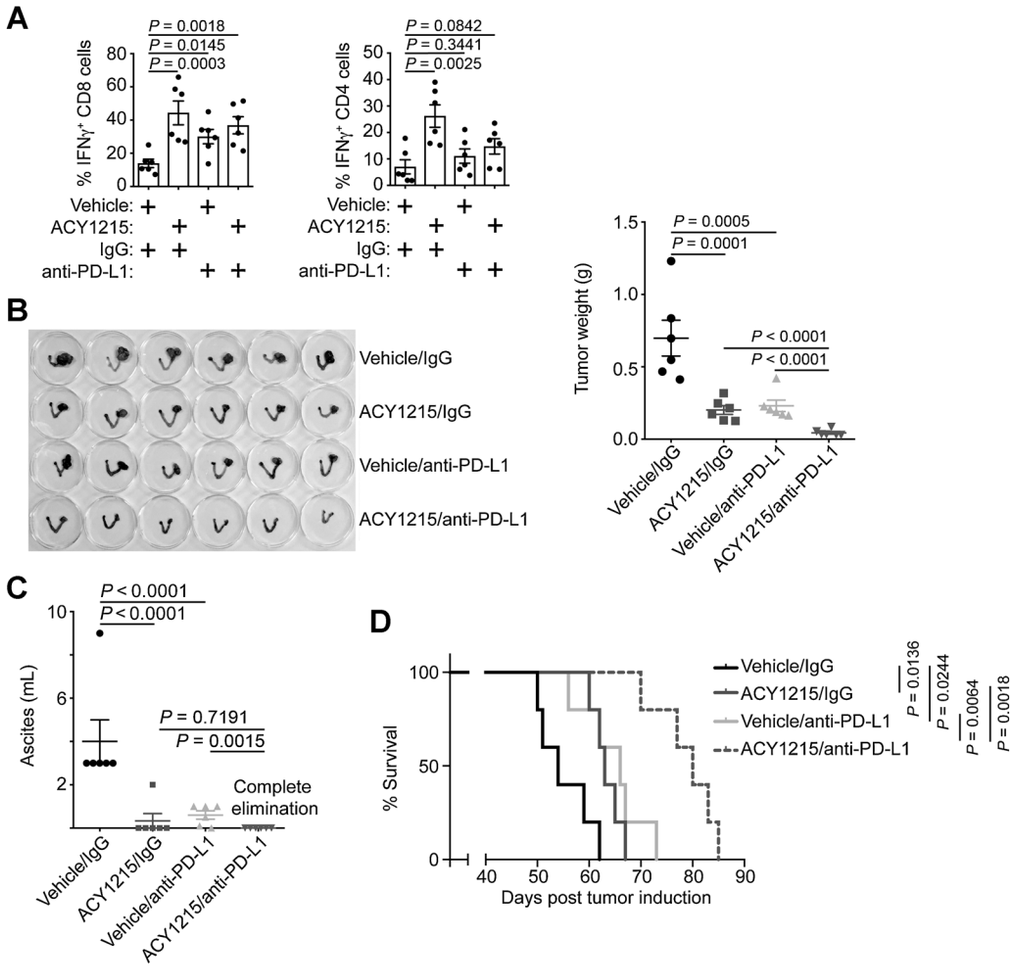

Figure 3.

ACY1215 and anti-PD-L1 are synergistic in limiting tumor progression *in vivo*. **A,** *ARID1A*$^{flox/flox}$/*PIK3CA*^{H1047R} OCCCs were induced by intrabursal adenovirus-encoded Cre injection and allowed to establish for 4 weeks. The mice were randomized into four indicated treatment groups and treated for an additional 3 weeks. At the end of treatment, percentage of IFNγ-positive CD8 and CD4 T cells was assessed by flow cytometry in the peritoneal wash. **B,** Six mice from each of the indicated groups were euthanized after treatment. Left, images of dissected reproductive tracks with tumors. Right, the weights of the dissected tumors were quantified as a surrogate for tumor burden. **C,** Same as **B**, but quantified for the ascites produced. **D,** After completing treatment, the mice were followed for survival, and the Kaplan–Meier survival curves for each of the indicated groups are shown. Error bars, ± SEM.

antibody significantly abrogated the observed reduction in tumor weight and ascites production induced by the combination (Fig. 4B). Consistently, the improvement of survival observed in the combination treatment group was also abrogated by the anti-CD8 antibody (Fig. 4C). However, anti-CD8 antibody did not significantly reduce the CD4 T-cell activation (Fig. 4D). This result indicates that T-cell activation induced by ACY1215 is not merely a reflection of reduction in tumor burden in the treated mice. Together, these results support that the observed antitumor effects in ARID1A-inactivated OCCCs by ACY1215 and anti-PD-L1 combination is CD8 cytotoxic T-cell dependent.

Discussion

Here we show that HDAC6 inhibitor, ACY1215, activates both CD4 and CD8 T cells and increases IFNγ$^+$ CD4 and CD8 T cells. In addition, HDAC6 inhibition suppresses the growth of *ARID1A*-mutated tumor in immunocompromised xenograft models (12). Thus, HDAC6 inhibitor may suppress *ARID1A*-mutated tumors by both targeting cancer cells and restoring antitumor immunity. The fact that depletion of CD8 T cells significantly abrogated the antitumor effects of HDAC6 inhibitor and anti-PD-L1 combination suggests that in this context the effects of the combination on tumor immune microenvironment played a major role in the observed antitumor effects.

Here we report that ARID1A directly represses *CD274* gene transcription. In addition, it has been reported that ARID1A inactivation created a mutator phenotype. Indeed, *ARID1A* mutation correlated with an increase in PD-L1 expression (9) and there was a trend toward improved response rate to checkpoint blockade in clear cell ovarian cancer, in which *ARID1A* is mutated in >50% of cases (24). Furthermore, there is evidence to suggest that

Downloaded from http://aacrjournals.org/cancerres/article-pdf/79/21/5482/2871694/5482.pdf by guest on 04 December 2023

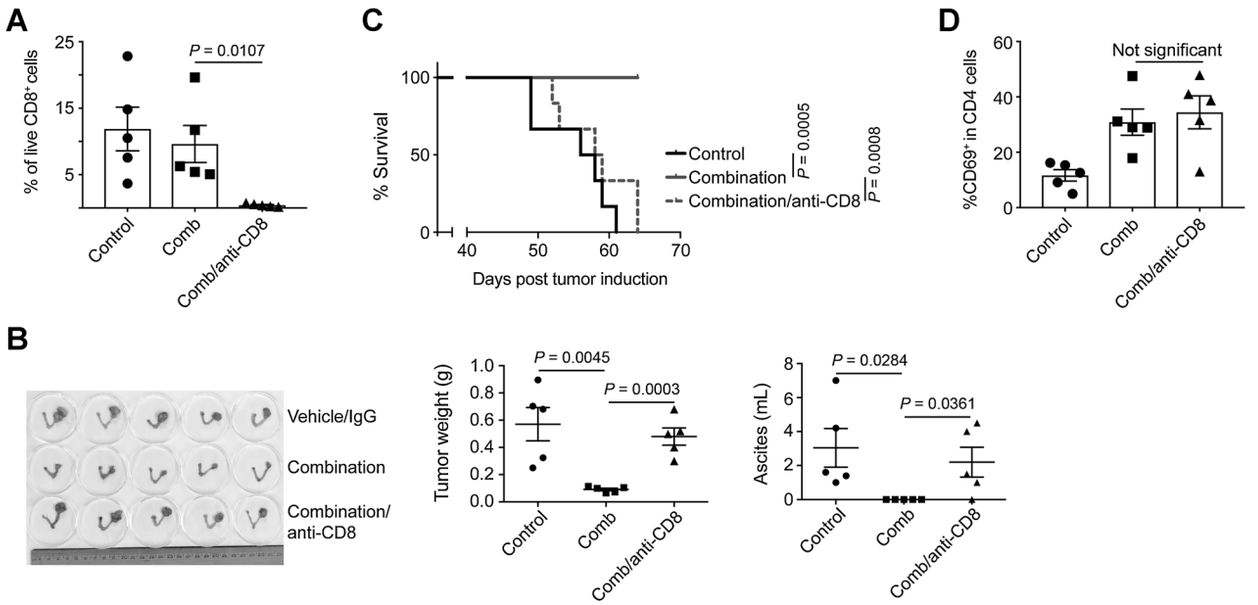

Figure 4.

Depletion of CD8$^+$ T cells abrogates the antitumor effects of ACY1215 and anti-PD-L1 combination. **A,** *ARID1A*$^{flox/flox}$/*PIK3CA*^{H1047R} OCCCs were induced by intrabursal adenovirus-encoded Cre injection and allowed to establish for 4 weeks. The mice were randomized into three indicated experimental groups ($n = 5$ mice/group). The depletion of CD8$^+$ T cells was confirmed by flow cytometry analysis of blood cells collected via the retro-orbital vein. **B,** Left, images of dissected reproductive tracks with tumors. The weights of the dissected tumors were quantified as a surrogate for tumor burden (middle), and ascites produced were quantified (right). **C,** After 3 weeks of treatment, the mice were followed for survival, and the Kaplan–Meier survival curves are shown. **D,** At the end of treatment, percentage of CD69-positive CD4 T cells was assessed by flow cytometry in the dissected tumors. Error bars, ± SEM.

inactivation of PBAF complex increased tumor cells sensitivity to IFNγ, resulted in enhanced secretion of chemokines that recruit effector T cells (7, 8). Thus, inactivation of ARID1A-containing BAF complex may increase PD-L1 expression directly at the *CD274* gene promoter or indirectly through increasing mutation loads. In addition, IFNγ appears to play a central role in regulating immune checkpoint and effector T-cell function by boosting PD-L1 expression when ARID1A-containing BAF complex is inactivated or through boosting IFNγ responsive genes when PBAF complex is inactivated (7, 8).

In summary, our findings identify a combination of HDAC6 inhibition and immune checkpoint blockade as an effective treatment strategy for ARID1A-inactivated tumors. Interestingly, *ARID1A* mutation predicts clinical response to pan-HDAC inhibition in urothelial carcinoma and specific HDAC6 inhibition was most potent in suppressing the growth of *ARID1A*-mutated urothelial cells (25). The HDAC6 inhibitor ACY1215 is now in clinical development for other cancer types, and anti-PD-L1 is FDA-approved. Thus, they are readily available for a combinational clinical application in *ARID1A*-mutated cancers.

Disclosure of Potential Conflicts of Interest

No potential conflicts of interest were disclosed.

Authors' Contributions

Conception and design: T. Fukumoto, R. Zhang
Development of methodology: T. Fukumoto, N. Fatkhutdinov, E.N. Tcyganov
Acquisition of data (provided animals, acquired and managed patients, provided facilities, etc.): T. Fukumoto, N. Fatkhutdinov, J.A. Zundell, E.N. Tcyganov, S. Karakashev, S. Wu, D.I. Gabrilovich
Analysis and interpretation of data (e.g., statistical analysis, biostatistics, computational analysis): T. Fukumoto, N. Fatkhutdinov, J.A. Zundell, E.N. Tcyganov, T. Nacarelli, S. Karakashev, S. Wu, Q. Liu
Writing, review, and/or revision of the manuscript: T. Fukumoto, N. Fatkhutdinov, E.N. Tcyganov, T. Nacarelli, S. Karakashev, Q. Liu, D.I. Gabrilovich, R. Zhang
Administrative, technical, or material support (i.e., reporting or organizing data, constructing databases): T. Fukumoto, N. Fatkhutdinov, S. Wu
Study supervision: R. Zhang

Acknowledgments

This work was supported by US NIH grants (R01CA160331, R01CA163377, R01CA202919, R01CA239128, and P50CA228991 to R. Zhang) and US Department of Defense (OC150446 and OC180109 to R. Zhang). The Honorable Tina Brozman Foundation for Ovarian Cancer Research (to R. Zhang) and Ovarian Cancer Research Alliance (Collaborative Research Development grant to R. Zhang and D.I. Gabrilovich), and Ann and Sol Schreiber Mentored Investigator Award (to S. Wu). Support of Core Facilities was provided by Cancer Centre Support Grant CA010815 to The Wistar Institute.

The costs of publication of this article were defrayed in part by the payment of page charges. This article must therefore be hereby marked *advertisement* in accordance with 18 U.S.C. Section 1734 solely to indicate this fact.

Received April 24, 2019; revised June 4, 2019; accepted July 9, 2019; published first July 16, 2019.

Downloaded from http://aacrjournals.org/cancerres/article-pdf/79/21/5482/2871694/5482.pdf by guest on 04 December 2023

References

1. Helming KC, Wang X, Roberts CWM. Vulnerabilities of mutant SWI/SNF complexes in cancer. Cancer Cell 2014;26:309–17.
2. Fukumoto T, Magno E, Zhang R. SWI/SNF complexes in ovarian cancer: mechanistic insights and therapeutic implications. Mol Cancer Res 2018; 16:1819–25.
3. Bailey MH, Tokheim C, Porta-Pardo E, Sengupta S, Bertrand D, Weerasinghe A, et al. Comprehensive characterization of cancer driver genes and mutations. Cell 2018;173:371–85.
4. Wiegand KC, Shah SP, Al-Agha OM, Zhao Y, Tse K, Zeng T, et al. ARID1A mutations in endometriosis-associated ovarian carcinomas. N Engl J Med 2010;363:1532–43.
5. Mackay HJ, Brady MF, Oza AM, Reuss A, Pujade-Lauraine E, Swart AM, et al. Prognostic relevance of uncommon ovarian histology in women with stage III/IV epithelial ovarian cancer. Int J Gynecol Cancer 2010;20: 945–52.
6. Jelinic P, Ricca J, Van Oudenhove E, Olvera N, Merghoub T, Levine DA, et al. Immune-active microenvironment in small cell carcinoma of the ovary, hypercalcemic type: rationale for immune checkpoint blockade. J Natl Cancer Inst 2018;110:787–90.
7. Miao D, Margolis CA, Gao W, Voss MH, Li W, Martini DJ, et al. Genomic correlates of response to immune checkpoint therapies in clear cell renal cell carcinoma. Science 2018;359:801–6.
8. Pan D, Kobayashi A, Jiang P, Ferrari de Andrade L, Tay RE, Luoma AM, et al. A major chromatin regulator determines resistance of tumor cells to T cell-mediated killing. Science 2018;359:770–5.
9. Shen J, Ju Z, Zhao W, Wang L, Peng Y, Ge Z, et al. ARID1A deficiency promotes mutability and potentiates therapeutic antitumor immunity unleashed by immune checkpoint blockade. Nat Med 2018;24:556–62.
10. Binnewies M, Roberts EW, Kersten K, Chan V, Fearon DF, Merad M, et al. Understanding the tumor immune microenvironment (TIME) for effective therapy. Nat Med 2018;24:541–50.
11. Veglia F, Perego M, Gabrilovich D. Myeloid-derived suppressor cells coming of age. Nat Immunol 2018;19:108–19.
12. Bitler BG, Wu S, Park PH, Hai Y, Aird KM, Wang Y, et al. ARID1A-mutated ovarian cancers depend on HDAC6 activity. Nat Cell Biol 2017;19:962–73.
13. Adeegbe DO, Liu Y, Lizotte PH, Kamihara Y, Aref AR, Almonte C, et al. Synergistic immunostimulatory effects and therapeutic benefit of combined histone deacetylase and bromodomain inhibition in non-small cell lung cancer. Cancer Discov 2017;7:852–67.
14. Woan KV, Lienlaf M, Perez-Villaroel P, Lee C, Cheng F, Knox T, et al. Targeting histone deacetylase 6 mediates a dual anti-melanoma effect: enhanced antitumor immunity and impaired cell proliferation. Mol Oncol 2015;9:1447–57.
15. Liu Y, Li Y, Liu S, Adeegbe DO, Christensen CL, Quinn MM, et al. NK cells mediate synergistic antitumor effects of combined inhibition of HDAC6 and BET in a SCLC preclinical model. Cancer Res 2018;78:3709–17.
16. Zhang Y, Kwon S, Yamaguchi T, Cubizolles F, Rousseaux S, Kneissel M, et al. Mice lacking histone deacetylase 6 have hyperacetylated tubulin but are viable and develop normally. Mol Cell Biol 2008;28:1688–701.
17. Santo L, Hideshima T, Kung AL, Tseng JC, Tamang D, Yang M, et al. Preclinical activity, pharmacodynamic, and pharmacokinetic properties of a selective HDAC6 inhibitor, ACY-1215, in combination with bortezomib in multiple myeloma. Blood 2012;119:2579–89.
18. Zhu H, Bengsch F, Svoronos N, Rutkowski MR, Bitler BG, Allegrezza MJ, et al. BET bromodomain inhibition promotes anti-tumor immunity by suppressing PD-L1 expression. Cell Rep 2016;16:2829–37.
19. Skene PJ, Henikoff JG, Henikoff S. Targeted in situ genome-wide profiling with high efficiency for low cell numbers. Nat Protoc 2018;13:1006–19.
20. Trizzino M, Barbieri E, Petracovici A, Wu S, Welsh SA, Owens TA, et al. The tumor suppressor ARID1A controls global transcription via pausing of RNA polymerase II. Cell Rep 2018;23:3933–45.
21. Helming KC, Wang X, Wilson BG, Vazquez F, Haswell JR, Manchester HE, et al. ARID1B is a specific vulnerability in ARID1A-mutant cancers. Nat Med 2014;20:251–4.
22. Pardoll DM. The blockade of immune checkpoints in cancer immunotherapy. Nat Rev Cancer 2012;12:252–64.
23. Chandler RL, Damrauer JS, Raab JR, Schisler JC, Wilkerson MD, Didion JP, et al. Coexistent ARID1A-PIK3CA mutations promote ovarian clear-cell tumorigenesis through pro-tumorigenic inflammatory cytokine signalling. Nat Commun 2015;6:6118.
24. Hamanishi J, Mandai M, Ikeda T, Minami M, Kawaguchi A, Murayama T, et al. Safety and antitumor activity of anti-PD-1 antibody, nivolumab, in patients with platinum-resistant ovarian cancer. J Clin Oncol 2015;33: 4015–22.
25. Gupta S, Albertson DJ, Parnell TJ, Butterfield A, Weston A, Pappas LM, et al. Histone deacetylase inhibition has targeted clinical benefit in ARID1A-mutated advanced urothelial carcinoma. Mol Cancer Ther 2019;18: 185–95.

Downloaded from http://aacrjournals.org/cancerres/article-pdf/79/21/5482/2871694/5482.pdf by guest on 04 December 2023